CHEMMEDCHEM

CHEMISTRY ENABLING DRUG DISCOVERY

Accepted Article

Title: Development of novel amides as non-covalent inhibitors of immunoproteasome

Authors: Roberta Ettari, Carmen Cerchia, Santina Maiorana, Manuela Guccione, Ettore Novellino, Alessandra Bitto, Silvana Grasso, Antonio Lavecchia, and Maria Zappalà

To be cited as: *ChemMedChem* 10.1002/cmdc.201900028

Link to VoR: http://dx.doi.org/10.1002/cmdc.201900028

A Journal of

ChemPubSoc Europe

WILEY-VCH

www.chemmedchem.org

Development of novel amides as non-covalent inhibitors of immunoproteasome

Roberta Ettari,[a]^ Carmen Cerchia,[b]^ Santina Maiorana,[a] Manuela Guccione,[a] Ettore Novellino,[b] Alessandra Bitto,[c] Silvana Grasso,[a] Antonio Lavecchia,*[b] Maria Zappalà*[a]

[a] Prof. R. Ettari 0000-0001-9020-2068, Dr. S. Maiorana, Dr. M. Guccione, Prof. S. Grasso 0000-0002-6368-0045, M. Zappalà 0000-0002-8942-797X
Departmentof Chemical, Biological, Pharmaceutical and Environmental Sciences
University of Messina
Viale Annunziata, 98168 Messina, Italy
E-mail: mzappala@unime.it

[b] Dr. C. Cerchia Prof. E. Novellino 0000-0002-2181-2142, Prof. A. Lavecchia 0000-0002-2181-8026,
Department of Pharmacy, "Drug Discovery" Laboratory
University of NapoliFederico II
Via Domenico Montesano 49, 80131 Napoli, Italy
E-mail: antonio.lavecchia@unina.it

[c] Prof. A. Bitto 0000-0001-9300-7532
Department of Clinical and Experimental Medicine
University of Messina
Via C. Valeria, 98125 Messina, Italy

^These authors contributed equally.

Abstract: The development of immunoproteasome-selective inhibitors is currently a promising strategy to treat hematologic malignancies, autoimmune and inflammatory diseases; in this context we now report the design, synthesis, and biological evaluation of a new series of amide derivatives as immunoproteasome inhibitors. Noteworthy, the designed compounds act as non-covalent inhibitors, which might be a promising therapeutic option because of the lack of all drawbacks and side-effects related to irreversible inhibition. Among all the synthesized compounds, we identified a panel of active inhibitors with K_i values in the low micromolar or submicromolar range towards β5i and/or β1i subunits of immunoproteasome. Within the active compounds, amide **7** proved to be the most potent and selective inhibitor with a K_i 21 nM against the sole β1i subunit. Docking studies allowed us to clarify the binding mode of the molecules in the catalytic site of immunoproteasome subunits.

Introduction

The 20S proteasome is the major non-lysosomal proteolytic system in eukaryotic cells, and it plays a key role in the degradation of most cellular proteins. Certain tumor cells are strongly dependent on proteasomal function, which however is at a normal level, while normal cells can better tolerate impairment of proteasome function; accordingly, proteasome inhibition in these cells represents a vulnerability that can be exploited to selectively kill tumor cells.[1-2] For these reasons, novel approaches of cancer therapy are based on proteasome inhibition. [3-5]

The central catalytic core 20S of 26S proteasome shows a barrel-like structure, with the two outer and the two inner rings composed of seven different α- and β-subunits, respectively. The catalytic subunits β1c, β2c and β5c, are responsible for the caspase-like (C-L), trypsin-like (T-L) and chymotrypsin-like (ChT-L) activities of the proteasome, respectively.[6]

Besides the constitutive proteasome (cCP), immunoproteasome (iCP) is a specialized form of vertebrates' proteasome, mainly represented in lymphocytes and monocytes. Under the stimuli of IFN-γ and TNF-α, β1c, β2c, and β5c subunits are replaced by β1i, β2i, and β5i subunits, respectively. Overall, substrate preference of β5i and β2i subunits overlaps with that of their cCP analogues, whereas β1i subunit reduces its caspase-like activity in favor of a chymotrypsin-like activity.[7]

High levels of immunoproteasome have been detected in a wide number of inflammatory diseases, such as Crohn's, inflammatory bowel and ulcerative diseases or in a panel of autoimmune diseases like rheumatoid arthritis or systemic lupus erythematosus.[8] On the other hand, iCPs are overexpressed in cells of hematopoietic origin, including multiple myeloma (MM) cells, thus targeting iCPs could be a valuable strategy for the treatment of this hematologic malignancy.[9-11] and, in this context, several β5i and/or β1i immunoproteasome selective inhibitors have been identified.[12-14]

Furthermore, in the last years, there have been some efforts to generate non-covalent proteasome/immunoproteasome inhibitors, thus providing important insights into the basic concepts of non-covalent proteasome inhibitor design.[15-18]

In this context, our research group has been actively involved in the development of novel 20S proteasome inhibitors;[19-24] in particular, we identified a series of amides,[21-23] some of which turned to be active against the ChT-L activity of 20S proteasome with K_i values in the submicromolar range. The non-covalent binding mode of the most active inhibitors was corroborated by docking simulations into the yeast 20S proteasome crystal structure.

With the aim to identify new immunoproteasome inhibitors, we first screened several amide derivatives, already synthesized in our laboratories, against the three immune subunits, i.e. β1i, β2i, β5i. Among the tested compounds, N-benzyl-2-(2-oxopyridin-1(2H)-yl)acetamide (**1**) proved to selectively inhibit β1i subunit with a *K*i of 2.23 μM; therefore, it was selected as hit compound to generate a series of analogues characterized by structural variations at the N-substituent and at the methylene linker between the pyridone scaffold and the amide function (Figure 1). Pyridones are frequently incorporated as peptidomimetic elements in protease inhibitors, including cysteine or serine proteases, being a suitable surrogate for a portion of the peptide or a convenient strategy to lock a defined conformation of the peptide.[25-27]

In particular, the amide group was functionalized with hydrophobic aliphatic or aromatic substituents (compounds **2-5**), in agreement to the structural features of the S1 pockets of β1i and β5i subunits that are large and hydrophobic, whereas the 2-pyridone at the P3 site was kept unchanged due to the nature of S3 subsite that is small and polar.[10] The glycine at P2 was replaced with a β-alanine homologue (compounds **6-11**), to evaluate if a longer distance between the amide portion and the pyridone scaffold could allow a better accommodation of these moieties into S1 and S3 pocket, respectively. The glycine residue at P2 was also replaced with a phenylalanine (compounds **12-18**), or with the homologous homophenylalanine (compounds **19-25**), in order to explore the size of the S2 pocket of the catalytic site of the immuno-subunits. With regard to the stereochemistry, compounds **12-25** have been developed in homochiral form with *S* absolute configuration, which appears to be the preferred one.

Noteworthy, the designed compounds lack of the electrophilic warhead and should act as non-covalent proteasome inhibitors that, with respect to covalent inhibitors, might be a promising alternative to use in therapy, because of the lack of all drawbacks and side-effects related to irreversible inhibition.[28]

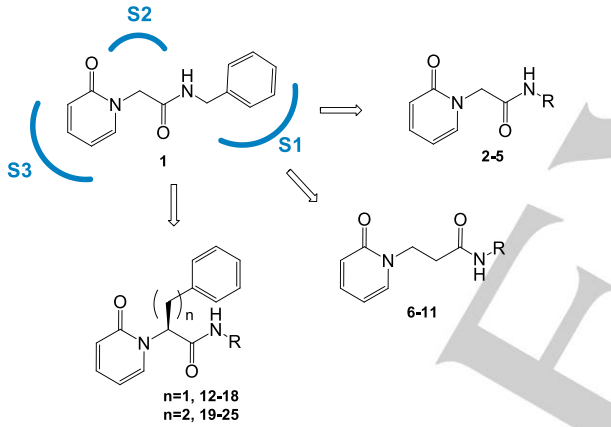

Figure 1. Structure of hit compound **1** and the new designed amide derivatives **2-25**.

Results and Discussion

Chemistry

The synthesis of amides **2-11** was achieved according to our previously reported procedure,[21] starting from 2(1*H*)-pyridone **26** that was *N*-alkylated with ethyl bromoacetate or methyl 3-bromopropionate in the presence of NaH, to give esters **27**-**28**. These latter intermediates were converted into the corresponding carboxylic acids **29**-**30** by alkaline hydrolysis with LiOH. Coupling reactions between the carboxylic acids **29**-**30** and the suitable amines, in the presence of EDC·HCl, HOBt, as coupling reagents, and DIPEA as a base, gave the desired amides **2-5** and **6-11** in good yields (Scheme 1).

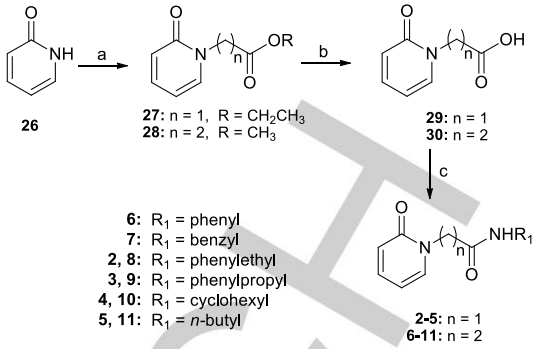

Scheme 1. Reagents and conditions**:** (a) NaH, DMF, 0°C, 1h, N_2; ethyl bromoacetate or methyl 3-bromopropionate, r.t. 12h; (b) LiOH, MeOH, 0°C-r.t., 6 h ; (c) DCM/DMF, 0°C, HOBt, EDC·HCl, 10 min, then DIPEA and a suitable amine, r.t., 12h.

The synthesis of the P2 fragments of compounds **12-25** was achieved starting from the commercially available (*R*)-2-hydroxy-3-phenyl propanoic acid methyl ester **31** and (*R*)-2-hydroxy-3-phenyl butanoic acid ethyl ester **32**, which were activated into the more reactive methanesulfonates **33-34,** by reaction with mesyl chloride in the presence of triethylamine (Scheme 2). Intermediates **33-34** were then condensed with the pyridone scaffold **26** to give the esters **35-36**, which were then converted into the corresponding carboxylic acids **37-38** by alkaline hydrolysis. Coupling reactions, carried out as reported in Scheme 1, between the carboxylic acids **37-38** and the suitable amines gave compounds **12-18** and **19-25** in high yields.

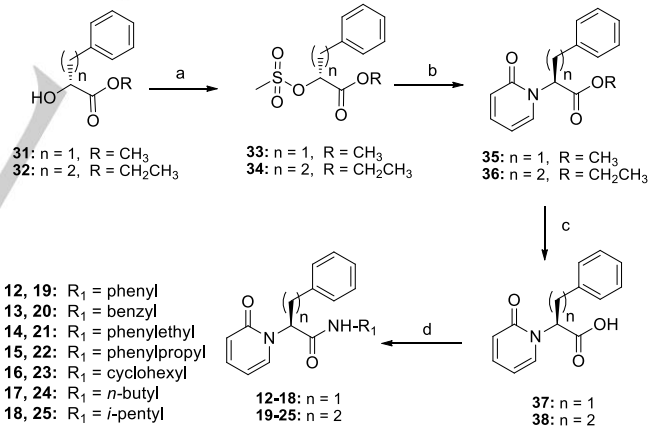

Scheme 2. Reagents and conditions**:** (a) MsCl, Et_3N, dry CH_2Cl_2, r.t., 2h, N_2; (b) compound **26**, NaH, dry DMF, 0°C-r.t., then **33** or **34**, 12h, N_2; (c) LiOH, MeOH/H_2O/dioxane (1:1:1), 0°C-r.t., 12h; (d) DMF, 0°C, HOBt, EDC·HCl, 10 min, then DIPEA and a suitable amine, 0°C-r.t., 12h.

Biological activity and docking studies

All the synthesized compounds were tested for their ability to inhibit each one of the catalytic subunits of c20S and i20S, by measuring the rate of hydrolysis of the appropriate fluorogenic substrate (Suc-Leu-Leu-Val-Tyr-AMC for β5i and β5c; Boc-Leu-Arg-Arg-AMC for β2i and β2c; Ac-Pro-Ala-Leu-AMC for β1i and Z-Leu-Leu-Glu-AMC for β1c). MG-132 (Z-Leu-Leu-Leu-al), a reversible inhibitor of both proteasome and immunoproteasome, was used as positive control.

First, compounds underwent a preliminary screening on each proteolytic subunit at 50 µM. Compounds able to inhibit the enzymatic activity by more than 60% were characterized in detail: Continuous assays were thus performed (progress curve method, at seven different concentrations, ranging from those that minimally inhibited to those that fully inhibited the immunoproteasome or the proteasome subunit) to determine the K_i values reported in Table 1.

Among all the tested compounds, some of them (i.e. **1, 7, 10-13, 19** and **21**) turned to be active on the iCPs. Interestingly, compounds **1** and **7,** which were *N*-benzyl substituted amides selectively inhibited the β1i subunit with a consistent improvement of activity observed for the *β*-alanine derivative with respect to the glycine derivative (K_i = 0.021 µM vs 2.23 µM).

The *β*-alanine derivatives **10** and **11**, bearing a cyclohexyl and an *n*-butyl substituent, on the contrary, targeted both the β1i and β5i subunits.

When a Phe residue was introduced at P2 site (e.g. compounds **12** and **13**), the activity was switched on both the constitutive and immuno-core particles (β5i and β5c), with a strong preference for the constitutive core-particle (see e.g. compound **12,** K_i = 8.81 µM and 45.5 µM for β5c and β5i, respectively).It is worth noting that, two the compounds bearing a HomoPhe residue at the P2 site turned to be active on both the ChT-L activities of i20S (i.e. **19**) or against the sole β5i (i.e. **21**).

Table 1. Activity on proteasome and immunoproteasome core-particles of compounds **1-25**.

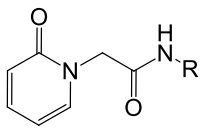

1-5

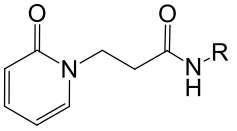

6-11

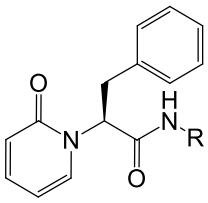

12-18

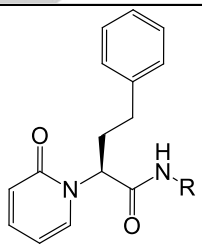

19-25

	% of inhibition at 50 µM or *K*i (µM)						
Comp.	R	β1c	β2c	β5c	β1i	β2i	β5i
1	benzyl	32%	21%	n.i.	2.23±0.26	17%	n.i.
2	phenylethyl	24%	n.i.	n.i.	44%	n.i.	n.i.
3	phenylpropyl	32%	n.i.	n.i.	n.i.	11%	n.i.
4	cyclohexyl	36%	n.i.	n.i.	22%	10%	3%
5	*n*-butyl	36%	n.i.	n.i.	n.i.	5%	n.i.
6	phenyl	23%	n.i.	25%	n.i.	11%	25%
7	benzyl	37%	n.i.	n.i.	0.021±0.002	25%	17%
8	phenylethyl	24%	n.i.	3%	27%	n.i.	46%
9	phenylpropyl	22%	n.i.	18%	37%	n.i.	15.17±0.63
10	cyclohexyl	23%	n.i.	12%	2.92±0.87	n.i.	5.74±0.63
11	*n*-butyl	19%	n.i.	4%	3.09±1.06	n.i.	14.29±3.0
12	phenyl	15%	6%	8.81±1.11	23%	n.i.	45.5± 2.6
13	benzyl	14%	8%	3.02±0.29	19%	n.i.	7.77±1.51
14	phenylethyl	10%	13%	20.4±2.2	10%	n.i.	43%
15	phenylpropyl	15%	12%	50%	25%	n.i.	45%
16	cyclohexyl	5%	6%	45%	16%	n.i.	39%
17	*n*-butyl	n.i.	n.i.	48%	30%	9%	33%
18	*i*-pentyl	8%	n.i.	55%	23%	n.i.	30%
19	phenyl	n.i.	23%	n.i.	5.9± 0.16	n.i.	5.81±0.37
20	benzyl	n.i.	26%	n.i.	21%	n.i.	38%
21	phenylethyl	n.i.	31%	n.i.	48%	14%	3.85± 0.46
22	phenylpropyl	n.i.	33%	n.i.	36%	4%	34%
23	cyclohexyl	n.i	30%	n.i.	40%	6%	42%
24	*n*-butyl	n.i.	31%	n.i.	29%	n.i.	37%
25	*i*-pentyl	n.i.	30%	17%	18%	6%	39%

[a] For Ki values, data represent the mean±SD of two independent determinations, each performed in duplicate. n.i.=no inhibition.

…

To help interpret the structure–activity relationship (SAR) data and elucidate the molecular mechanism of i20S inhibition of the most active compounds **1**, **7**, **13** and **21**, docking studies were carried out using the GOLD Suite docking package[29] with the X-ray crystal structure of the murine i20S in complex with the epoxyketone inhibitor PR-957 (PDB: 3UNF).[10] This structure was selected due to the high degree of amino acid sequence identity (>90%) between mouse and human i20S subunits around the respective catalytic sites. Moreover, the few non-identical residues are located at the interface with the concomitant adjacent subunits and are thus absent from the catalytic sites. Furthermore, the crystal structure of PR-957 bound to β1i reveals two well-defined water molecules within the S3 pocket, which coordinate a tight H-bond network between β1i-A50N, β2i-S118Oγ and the backbone amide nitrogen and carbonyl oxygen of the P3 alanine residue of PR-957. Accordingly, the intervening water molecules were included in the docking experiments.

Docking of the amide derivative **1** to the β1i subunit revealed a binding mode similar to that of PR-957 (Fig. 2a), with an almost identical positioning of the backbone amides, the P1 phenyl moieties adopting the same spatial arrangement and the P3 alanine residue of PR-957 nicely overlapped with the pyridone ring of **1** (Fig. 2b). The P1 benzyl substituent extends deeply into the S1 pocket, forming hydrophobic contacts with V20, F31, L45, A49 and A52. The **1** backbone amide in engaged in H-bonds with the NH group of S21 backbone and the carbonyl oxygen of G47 backbone, whereas the carbonyl oxygen of the pyridone ring accepts further H-bonds from A49N, S48O$^{\gamma}$ and A50N, these last two through one of the two intervening water molecules located crystallographically in the PR-957 structure and included in our model. Moreover, the second water molecule forms a H-bond with the first one, while simultaneously engaging the β2i-S11833O$^{\gamma}$, which is at the bottom of the S3 pocket and contributes to a further stabilization of the ligand into the active site. Additional hydrophobic interactions occur between the pyridone ring and the V20 and V27 side chains located in proximity of S3 pocket of β1i subunit.

The β1i and β1c subunits strongly differ in their amino acid lining in the unprimed substrate binding channel. The hydrophobic active site surrounding of subunit β1i is replaced by a more polar one in subunit β1c. In particular, the amino acid substitutions V20T, F31T, L45R and A52T increase the polarity and the size of the β1c S1 pocket. Therefore, the more hydrophilic S1 pocket of subunit β1c opposes binding of the hydrophobic P1 substituents. These findings are in agreement with the poor inhibitory activity displayed by this series of derivatives towards β1c.

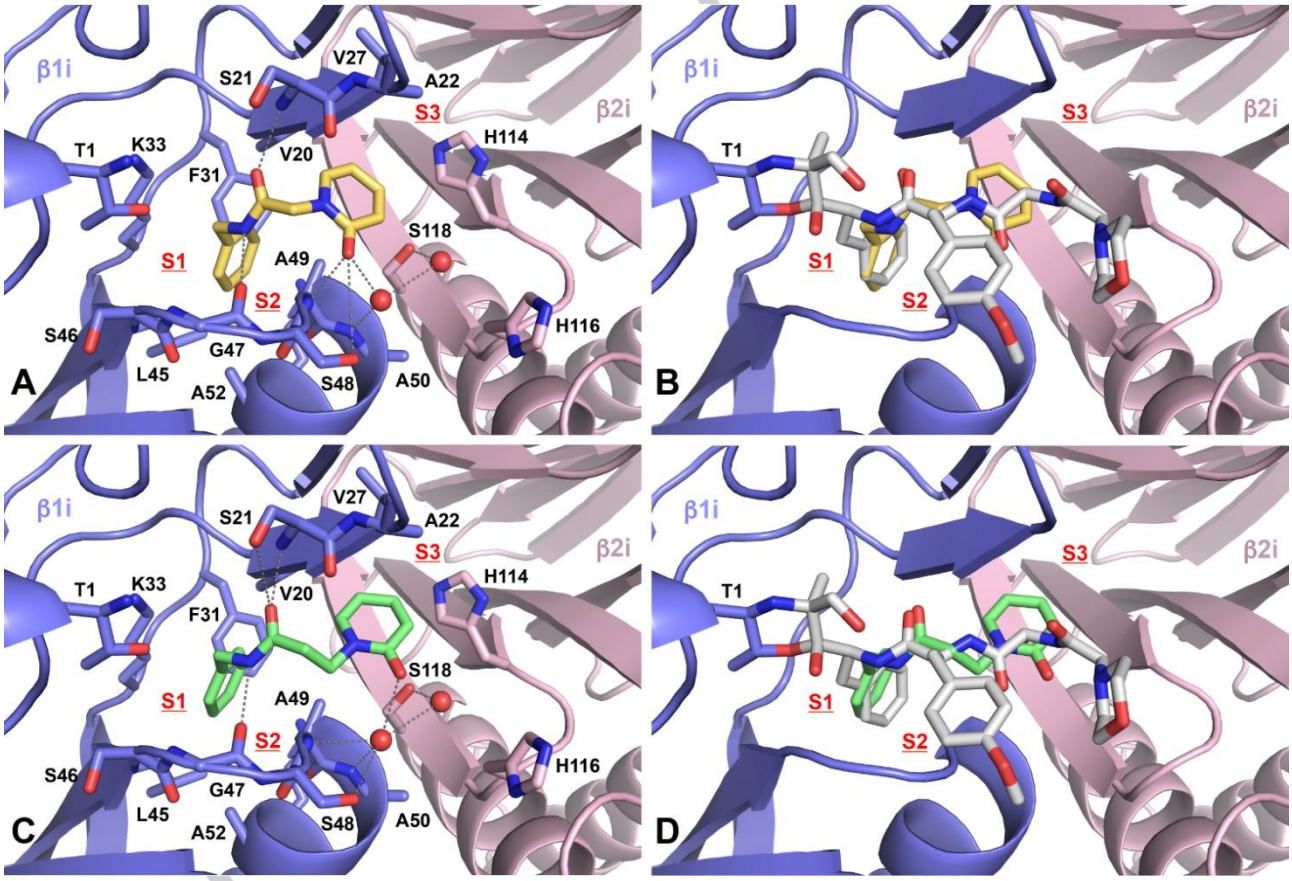

Figure 2. Binding modes of compounds **1** (A, yellow orange sticks) and **7** (C, lime green sticks) into the β1i (slate)/β2i (light pink) active site of mouse i20S, represented as a ribbon model. Only amino acids located within 4 Å of the bound ligand are displayed and labelled. H-bonds discussed in the text are depicted as dashed grey lines. The defined water molecules forming tight H-bonds to the protein are displayed as red spheres. S1-S3 specificity pockets are labeled. An overlay of **1** (B, docked pose) and **7** (D, docked pose) with PR-957 (white sticks, X-ray crystal pose) is shown in the β1i/β2i active site of mouse i20S.

Elongation of the linker between the pyridone ring and the amide function from one to two methylene units yielded compound **7**, which showed the highest inhibitory potency and selectivity towards β1i (K_i = 0.021 μM). As a result of the docking of **7** into the β1i subunit, we obtained a complex showing an overall binding mode similar to that of **1** (Fig. 2c,d), with the ligand forming H-bonds with G47O, S21N and S21O$^{\gamma}$ of β1i through the amide group as well as the same pattern of hydrophobic interactions within the S1 pocket. These results are in consonance with the SAR data showing that compounds bearing a benzyl (**7**), cyclohexyl (**10**) or *n*-butyl (**11**) residue at P1 inhibit β1i much stronger than β1c, which confirms that the S1 pocket of β1i is more hydrophobic than that of β1c.[7] In addition, neither β1i nor β1c is inhibited by compounds featuring a bulky phenylethyl (**8**) or phenylpropyl (**9**) substituent at P1, an outcome that supports structural data displaying that β1i/c have a smaller S1 pocket than β5i/c.[10]

The pyridone moiety of **7** fits into the S3 pocket formed by S48, S118 and H114, which is beneficial for improving potency and selectivity for β1i subunit (Fig. 2c). In particular, the pyridone carbonyl oxygen forms a tight H-bond network with A49N, S48Oγ and A50N of β1i through one water molecule and with β2i-S118Oγ via the second water molecule. Additionally, the aromatic pyridone core makes an edge-to-face π-stacking interaction with the H114 imidazole ring in the subunit β2i. Compared to β1c, the S3 pocket of β1i is characterized by the amino acid replacements T22A, A27V as well as Y114H in the neighbouring subunit β2i. These differences lead to a more size-restricted and more hydrophilic S3 pocket in β1i compared to its counterpart β1c.

A second series of derivatives was designed, in which a residue of phenylalanine was used to replace the glycine P2 group. Among them, compound **13** was moderately active against β5i (K_i = 7.77 μM) and displayed a fairly good potency against β5c (K_i = 3.02 μM). As depicted in Fig. 3a,b, **13** exhibited a binding mode in β5i similar to that of derivatives **1**, **7** and PR-957. The P1 benzyl substituent fits into the S1 pocket, the backbone amide is stabilized by H-bonds with G47O, T21N and T21O$^{\gamma}$ of β5i and the pyridone group protrudes into the S3 site with the carbonyl engaged in H-bonds with A49N and C48S. The P2 phenylalanine moiety projects into the central core of the 20S cavity, making little or no contacts with the β5i subunit. Docking of **13** to the human c20S crystal structure[30] elucidates that the P1 benzyl and the P3 pyridone ring fit into subunit β5c by interacting with T21, A27, A49, S129 and D144 of the neighbouring subunit β6 via an intervening water molecule. This latter interaction stabilizes the ligand into the S3 pocket and accounts for the enhanced potency of **13** for β5c.

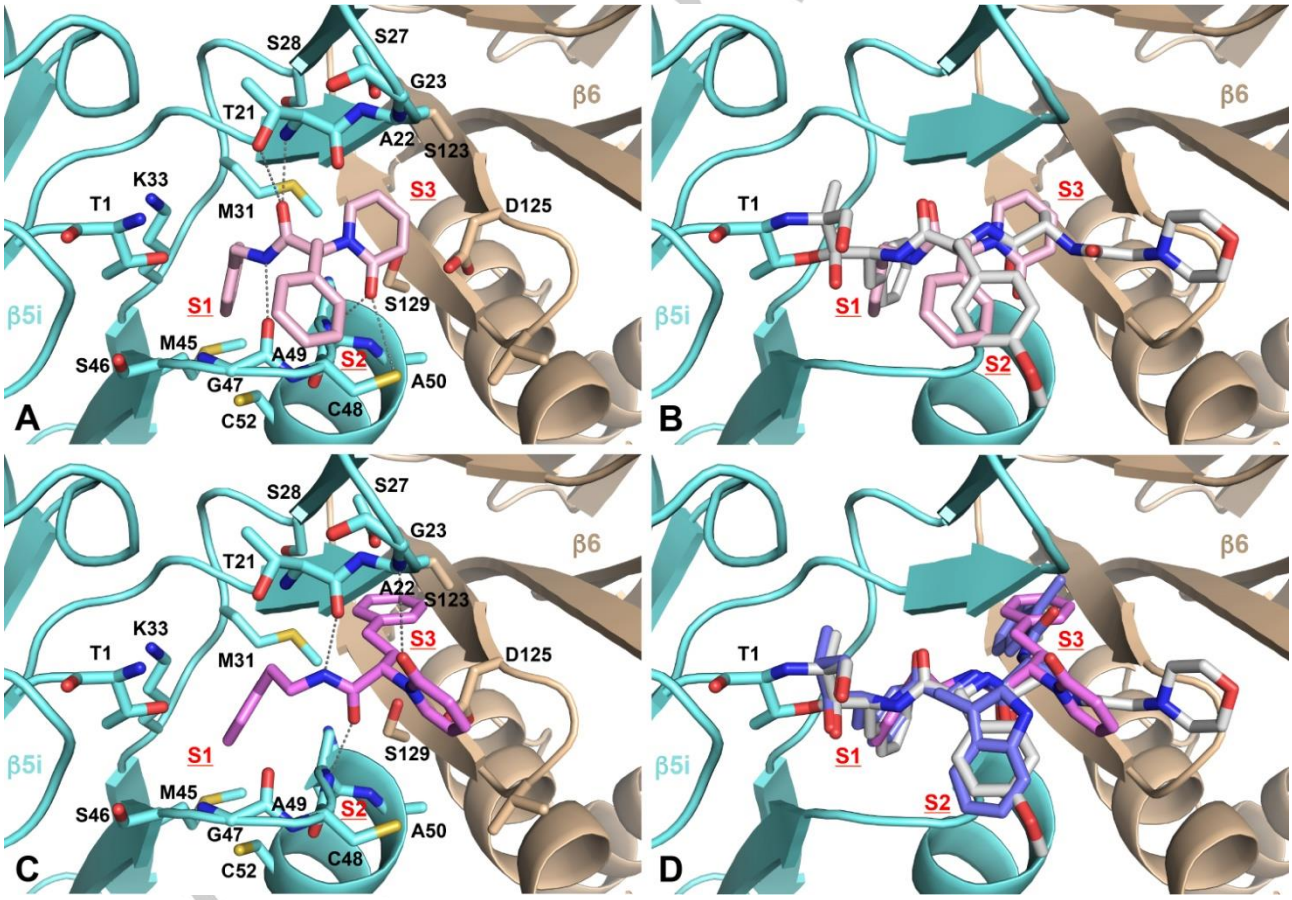

Figure3. Binding modes of compounds **13** (A, pink sticks) and **21** (C, violet) into the β5i (aquamarine)/β6 (wheat) active site of mouse i20S, represented as a ribbon model. Only amino acids located within 4 Å of the bound ligand are displayed and labelled. H-bonds discussed in the text are depicted as dashed grey lines. S1-S3 specificity pockets are labeled. An overlay of **13** (B, docked pose) and **21** (D, docked pose) with PR-957 (white sticks, X-ray crystal pose) is shown in the β5i/β6 active site of mouse immunoproteasome. Compound **21** overlaps with the X-ray crystal pose of PR-924 (slate sticks) bound to the humanized yeast i20S (PDB: 5L5H).

Noteworthy, substitution of the glycine residue at P2 with a homophenylalanine residue yielded a series of derivatives in which the activity against c20S subunits β1 and β5 was completely lost. Among them, compound **21** showed selective inhibitory activity against β5i (K_i = 3.85 μM). Docking of **21** into the subunit β5i revealed a different binding mode in comparison to **1** and **7** derivatives, with the P2 substituent protruding into the S3 subsite instead of pointing toward the initially assumed S2 binding pocket (Fig. 3c). As a consequence, the pyridone scaffold assumes a folded conformation, engaging a very weak H-bond with β5i-G23N (distance of 4 Å).[31] The backbone amide establishes a H-bonding network involving T21O and A49N. The homophenylalanine residue deeply extends into the S3 subsite making O-H/π interactions with the hydroxyl groups of S27 from β5i and S129 from β6. The phenylethyl at P1 perfectly fits into the spacious S1 pocket of β5i and is stabilized by a cation-π contact with K33, a sulfur–arene interaction with M45[32-33] and by C-H/ π interactions with the side chains of M31, K33, and A49. Interestingly, the overlay of the docked pose of **21** with the β5i-specific inhibitors PR-957 (PDB ID: 3UNF) and PR-924 bound to the chimeric hβ5/hβ6 substrate binding channel (PDB ID: 5L5H)[34] reveals that **21** and PR-924 adopt a similar kinked binding mode, with an identical positioning of the amide scaffolds and a similar orientation of the P1 and P3 functions, whereas PR-957 adopts a linear orientation (Fig. 3d). The superior β5i-selectivity of **21** compared to ligands that target the strictly conserved peptide binding sites seems to result from its ability to exploit subpockets other than the substrate-binding channels. Moreover, insights into the selectivity of **21** towards i20S over c20S can be gained when considering amino acid compositions of β5c and β5i S1 pockets. Although the S1 specificity pockets of both β5c and β5i are formed by the same residues, the conformation of M45 in β5c is different from that in β5i, thus resulting in peculiarly sized S1 specificity pockets.[7] The observed selectivity of **21** can be rationalized by the impaired accommodation of the phenylethyl moiety into the smaller β5c S1 pocket because of the closed conformation of M45.

Conclusions

In conclusions, with our work we identified a series of amides with K_i values in the low micromolar or submicromalar range towards one or two chymotrypsin-like activities of immunoproteasome (β5i and β1i subunits). Amide **7** was identified as lead compound, due to the selective inhibition of β1i subunit in the submicromolar range (K_i = 21 nM).

Docking studies allowed us to clarify the binding mode of the amides in the catalytic site of immunoproteasome proteolytic subunits, thus explaining the preferential inhibition of immunoproteasome with respect to proteasome.

Worthy of note, the non-covalent inhibition, characteristic of our amides, is strongly desirable, because free of drawbacks and side-effects related to covalent inhibition. Our future efforts will be devoted to optimize the identified lead compound **7** in terms of potency and selectivity and to check activity against a panel of hematological malignancies or against autoimmnune diseases, because controversial data are currently reported in literature related to the specific proteasome inhibition in MM cells and disease models.[35,36]

Experimental Section

Materials & methods

Chemistry.

All reagents and solvents were purchased from commercial suppliers and used without any further purification. Elemental analyses were performed on a C. Erba Model 1106 Elemental Analyzer and the results are within ±0.4% of the theoretical values. Merck silica gel 60 F254 plates were used for analytical TLC; column chromatography was carried out on Merck silica gel (200–400 mesh). ^{1}H-NMR and ^{13}C-NMR spectra were recorded on a Varian 300 MHz NMR spectrometer operating at frequencies of 300.13 and 75.47 MHz, or on a Varian 500 MHz spectrometer operating at 499.74 and 125.73 MHz for ^{1}H-NMR and ^{13}C-NMR spectra, respectively. The residual signal of the deuterated solvent was used as internal standard. Chemical shifts are given in δ (ppm) and coupling constants (*J*) in Hz. Splitting patterns are described as singlet (s), broad singlet (bs), doublet (d), triplet (t), quartet (q), multiplet (m), doublet of doublet (dd), or triplet of doublets (td). Compounds **27-30** were synthesized as previously reported.[20, 23].

General procedures for the synthesis of amides 2-5 and 6-11

The coupling reactions between the carboxylic acid (**29** or **30**) (1 equiv.) and the appropriate amines (1.5 equiv.) were carried out by dissolving compound **29** or **30** in dry DMF, then cooling to 0°C and adding HOBt (1.5 equiv.) and EDC·HCl (1.5 equiv.). After 10 minutes, DIPEA (2 equiv.) and the amine (1.5 equiv.) dissolved in DMF were added dropwise, and the mixture was stirred at room temperature overnight. The organic layer was washed with brine, dried over Na_2SO_4, filtered and concentrated under reduced pressure. The crude residue were purified by column chromatography, using $CHCl_3$/MeOH, 95:5 as eluent mixture.

2-(2-Oxopyridin-1(2*H*)-yl)-*N*-phenethylacetamide (2): yield: 90%. R_f = 0.32 ($CHCl_3$/MeOH, 95:5). ^{1}H NMR (300 MHz, $CDCl_3$): δ = 2.78 (t, J = 7.1 Hz, 2H), 3.48 (q, J = 7.1 Hz, 2H), 4.49 (s, 2H), 6.25 (td, J = 6.6, 1.4 Hz, 1H), 6.60 (d, J = 9.1 Hz, 1H), 6.92 (bs, 1H), 7.12 (d, J = 7.1 Hz, 2H), 7.18-7.28 (m, 3H), 7.34-7.44 (m, 2H) ppm. ^{13}C NMR (75 MHz, $CDCl_3$): δ = 35.45, 40.80, 54.02, 107.02, 120.85, 126.42, 128.54, 128.66, 130.75, 137.98, 140.50, 162.81, 167.25 ppm. Elemental analysis: calcd for $C_{15}H_{16}N_2O_2$: C 70.29, H 6.29, N10.93; found: C 70.11, H5.98, N 11.17.

2-(2-Oxopyridin-1(2*H*)-yl)-*N*-(3-phenylpropyl)acetamide (3): yield: 85%. R_f = 0.50 ($CHCl_3$/MeOH, 95:5). ^{1}H NMR (300 MHz, $CDCl_3$): δ = 1.76-1.86 (m, 2H), 2.59 (t, J = 7.6 Hz, 2H), 3.24 (q, J = 6.9 Hz, 2H), 4.52 (s, 2H), 6.27 (td, J = 6.6, 1.1 Hz, 1H), 6.63 (dd, J = 9.6, 1.1 Hz, 1H), 7.04 (bs, 1H), 7.1-7.31 (m, 5H), 7.38-7.45 (m, 2H) ppm. ^{13}C NMR (75 MHz, $CDCl_3$): δ = 30.85, 33.02, 39.14, 53.77, 106.99, 120.62, 125.91, 128.34, 138.37, 140.64, 141.30, 162.87, 167.10 ppm. Elemental analysis: calcd for $C_{16}H_{18}N_2O_2$: C 71.09, H 6.71, N 10.36; found: C 71.32, H 6.43, N 10.68.

***N*-Cyclohexyl-2-(2-oxopyridin-1(2*H*)-yl)acetamide (4):** yield: 65%. R_f = 0.60 ($CHCl_3$/MeOH, 95:5). ^{1}H NMR (300 MHz, $CDCl_3$): δ = 1.06-1.90 (m, 10H), 3.62-3.74 (m, 1H), 4.49 (s, 2H), 6.25 (td, J = 6.7, 1.3 Hz, 1H), 6.61 (d, J = 8.8 Hz, 1H), 6.81 (bs, 1H), 7.34-7.45 (m, 2H) ppm. ^{13}C NMR (75 MHz, $CDCl_3$): δ = 24.58, 25.40, 32.55, 48.45, 53.45, 106.76, 120.45, 138.55, 140.52, 162.80, 166.05 ppm. Elemental analysis: calcd for $C_{13}H_{18}N_2O_2$: C 66.64, H 7.74, N 11.96; found: C 66.89, H 7.86, N 11.74.

***N*-Butyl-2-(2-oxopyridin-1(2*H*)-yl)acetamide (5):** yield: 44%. R_f = 0.24 ($CHCl_3$/MeOH, 95:5). ^{1}H NMR (300 MHz, $CDCl_3$): δ = 0.89 (t, J = 7.2 Hz, 3H), 1.24-1.36 (m, 2H), 1.40-1.52 (m, 2H), 3.21 (q, J = 7.2, 2H), 4.53 (s, 2H), 6.25 (td, J = 6.7, 1.3 Hz, 1H), 6.63 (dd, J = 9.8, 1.3 Hz, 1H), 6.93 (bs, 1H), 7.36-7.45 (m, 2H) ppm. ^{13}C NMR (75 MHz, $CDCl_3$): δ = 13.67, 19.96, 31.25, 39.35, 53.59, 106.88, 120.56, 138.43, 140.56, 162.84, 166.99 ppm. Elemental analysis: calcd for $C_{11}H_{16}N_2O_2$: C 63.44, H 7.74, N13.45; found: C 63.61, H 7.53, N 13.64.

3-(2-Oxopyridin-1(2*H*)-yl)-*N*-phenylpropanamide (6): yield: 62%. R_f= 0.43 ($CHCl_3$/MeOH 95:5). ^{1}H NMR (300 MHz, CDCl3): δ = 2.96 (t, J = 5.8 Hz, 2H), 4.34 (t, J = 5.8 Hz, 2H), 6.19 (td, J = 6.7, 1.2 Hz, 1H), 6.45 (d, J = 9.0 Hz, 1H), 7.07 (t, J = 7.4 Hz, 1H), 7.24-7.36 (m, 3H), 7.53-7.66 (m, 3H), 9.78 (bs, 1H) ppm.^{13}C NMR (75 MHz, $CDCl_3$): δ = 32.76, 45.21, 111.73, 118.92, 121.65, 124.45, 129.08, 134.52, 138.41, 138.87, 161.71, 173.73 ppm. Elemental analysis: calcd for $C_{14}H_{14}N_2O_2$, C 69.41, H 5.82, N 11.56; found. C 69.28, H 5.91, N 11.46.

***N*-Benzyl-3-(2-oxopyridin-1(2*H*)-yl)propanamide (7):** yield: 46%. R_f = 0.42 ($CHCl_3$/MeOH, 95:5). ^{1}H NMR (300 MHz, $CDCl_3$): δ = 2.74 (t, J = 6.1 Hz, 2H), 4.21 (t, J = 6.1 Hz, 2H), 4.38 (d, J = 5.8 Hz, 2H), 6.12 (td, J = 6.8, 1.2 Hz, 1H), 6.38 (d, J = 9.1 Hz, 1H), 6.81 (bs, 1H), 7.14 (d, J = 7.1 Hz, 2H), 7.22-7.32 (m, 4H), 7.43 (dd, J = 6.8, 1.6 Hz, 1H) ppm. ^{13}C NMR (125.73 MHz, $CDCl_3$): δ = 34.99, 43.49, 47.17, 106.13, 120.43, 127.35, 127.62, 128.56, 138.04, 139.10, 139.97, 162.77, 169.93 ppm. Elemental analysis: calcd for $C_{15}H_{16}N_2O_2$: C 70.29, H 6.29, N10.93; found: C 70.56, H 6.46, N 10.62.

3-(2-Oxopyridin-1(2*H*)-yl)-*N*-phenethylpropanamide (8): yield: 33%. R_f = 0.34 ($CHCl_3$/MeOH, 95:5). ^{1}H NMR (500 MHz, $CDCl_3$): δ = 2.66 (t, J = 6.4 Hz, 2H), 2.74 (t, J = 7.0 Hz, 2H), 3.47 (q, J = 7.0 Hz, 2H), 4.22 (t, J = 6.4 Hz, 2H), 5.81 (bs, 1H), 6.16 (t, J = 6.4 Hz, 1H), 6.55 (d, J =9.1 Hz, 1H), 7.11 (d, J = 7.1 Hz, 2H), 7.19-7.38 (m, 4H), 7.44 (dd, J = 6.4, 1.6 Hz, 1H) ppm. ^{13}C NMR (125.73 MHz, $CDCl_3$): δ = 35.14, 35.55, 40.73, 46.94, 105.98, 120.61, 126.50, 128.64, 128.61, 138.62, 139.01, 139.93, 162.75, 169.92 ppm. Elemental analysis: calcd for $C_{16}H_{18}N_2O_2$: C 71.09; H 6.71; N 10.36; found: C 71.39, H 6.56, N 6.96.

3-(2-Oxopyridin-1(2*H*)-yl)-*N*-(3-phenylpropyl)propanamide (9): yield: 33%. R_f =0.34 ($CHCl_3$/MeOH, 95:5). ^{1}H NMR (500 MHz, $CDCl_3$): δ = 1.72-1.78 (m, 2H,), 2.55 (t, J = 7.7 Hz, 2H), 2.67 (t, J = 6.1 Hz, 2H), 3.22 (q, J = 6.8 Hz, 2H), 4.21 (t, J = 6.1 Hz, 2H), 6.12 (td, J = 6.7, 0.8 Hz, 1H), 6.45 (bs, 1H), 6.49 (d, J = 9.1 Hz, 1H), 7.1-7.26 (m. 5H), 7.30 (ddd, J = 9.1, 6.7, 1.9 Hz, 1H), 7.43 (dd, J = 6.7, 1.5 Hz, 1H) ppm. ^{13}C NMR (125.73 MHz, $CDCl_3$): δ = 30.98, 33.14, 35.14, 39.18, 47.05, 106.11, 120.44, 125.94, 128.30, 128.39, 139.09, 140.05, 141.36, 162.79, 169.95 ppm. Elemental analysis: calcd for $C_{17}H_{20}N_2O_2$: C 71.81; H 7.09; N 9.85; found: C 71.45, H 7.21, N 9.73.

***N*-Cyclohexyl-3-(2-oxopyridin-1(2*H*)-yl)propanamide (10):** yield: 36%. R_f = 0.41 ($CHCl_3$/MeOH, 95:5). ^{1}H NMR (500 MHz, $CDCl_3$): δ = 0.98-1.83 (m, 10H), 2.67 (t, J = 6.1 Hz, 2H), 3.61-3.72 (m, 1H), 4.22 (t, J = 6.1 Hz, 2H), 6.07 (bs, 1H), 6.15 (td, J = 6.7, 1.2 Hz, 1H), 6.52 (d, J = 9.1 Hz, 1H), 7.34 (ddd, J = 9.1, 6.7, 2.0 Hz, 1H), 7.43 (dd, J = 6.7, 1.6 Hz, 1H) ppm. ^{13}C NMR (125.73 MHz, $CDCl_3$): δ = 24.78, 25.41, 32.89, 35.37, 47.19, 48.28, 105.97, 120.48, 139.08, 139.93, 162.78, 168.93 ppm. Elemental analysis: calcd for $C_{14}H_{20}N_2O_2$: C, 67.71; H, 8.12; N, 11.28; found: C 67.94, H 7.93, N 11.55.

***N*-Butyl-3-(2-oxopyridin-1(2*H*)-yl)propanamide (11):** yield: 57%. R_f = 0.37 ($CHCl_3$/MeOH, 95:5). ^{1}H NMR (500 MHz, $CDCl_3$): δ = 0.87 (t, J = 7.3 Hz, 3H), 1.21-1.30 (m, 2H), 1.37-1.44 (m, 2H), 2.70 (t, J = 6.1 Hz, 2H), 3.19 (q, J = 7.0, 2H), 4.23 (t, J = 6.1 Hz, 2H), 6.16 (td, J = 6.7, 1.1 Hz, 1H), 6.40 (bs, 1H), 6.50 (d, J = 9.1 Hz, 1H), 7.34 (ddd, J = 9.1, 6.7, 2.0 Hz, 1H), 7.45 (dd, J = 6.7, 1.6 Hz, 1H) ppm. ^{13}C NMR (125.73 MHz, $CDCl_3$): δ = 13.66, 19.93, 31.45, 35.14, 39.26, 47.10, 106.04, 120.43, 139.10, 139.97, 162.78, 169.87 ppm. Elemental analysis: calcd for $C_{12}H_{18}N_2O_2$: C 64.84; H 8.16; N 12.60; found: C 64.55, H 7.78, N 12.77.

Synthesis of carboxylic acids 37-38

(*R*)-1-(Methoxycarbonyl)-2-phenylethyl methanesulfonate (33) A solution of **31** (1.2 g, 6.6 mmol) in dry DCM was reacted with methanesulfonyl chloride (1.5 g, 13.2 mmol, 1.02 mL) and Et_3N (1.67 g, 16.5 mmol, 2.29 mL). The mixture was stirred at room temperature under nitrogen for 2 hours, then washed with water and dried (Na_2SO_4), filtered and evaporated under reduced pressure to afford **33** as a brown/yellow oil. Yield: 1.68 g (99%); R_f = 0.73 (light petroleum/EtOAc, 4:6). ^{1}H NMR (300 MHz, $CDCl_3$): δ = 2.77 (s, 3H), 3.12 (dd, *J* = 14.4, 8.8 Hz, 1H), 3.31 (dd, *J* = 14.4, 4.2 Hz, 1H), 3.80 (s, 3H), 5.18 (dd, *J* = 8.8, 4.2 Hz, 1H), 7.23-7.37 (m, 5H) ppm.

(*R*)-1-(Ethoxycarbonyl)-3-phenylpropyl methanesulfonate (34) According to the same procedure described for **33,** compound **32 (**1 g, 4.8 mmol, 0.930 mL) was reacted with methanesulfonyl chloride (1.01 g, 9.6 mmol, 0.74 mL) and Et_3N (1.21 g, 12 mmol, 1.67 mL) to give the title compound **34** as a brown/yellow oil. Yield: 1.4 g (99%); R_f = 0.77 (light petroleum/EtOAc, 4:6). ^{1}H NMR (300 MHz, $CDCl_3$): δ = 1.29 (t, *J* = 7.2 Hz, 3H), 2.18-2.30 (m, 2H), 2.75-2.83 (m, 2H) 3.17 (s, 3H), 4.23 (q, *J* = 7.2 Hz, 2H), 5.02 (dd, *J* = 7.8, 4.7 Hz, 1H), 7.17-7.35 (m, 5H) ppm.

(*S*)-Methyl 2-(2-oxopyridin-1(2*H*)-yl)-3-phenylpropanoate (35). To a suspension of NaH (311.7 mg, 7.8 mmol) in dry DMF, at 0 ºC under N_2, a solution of pyridin-2(1H)-one **26** (741 mg, 7.8 mmol) in dry DMF was added via syringe. After stirring for 1h, (*R*)-1-(methoxycarbonyl)-2-phenylethyl methanesulfonate **33** (1.68 g, 6.5 mmol) was added to the mixture and the reaction was stirred overnight at room temperature. The reaction was then quenched with saturated NH_4Cl and the product was extracted with EtOAc. The combined organic layers were washed with brine, dried over Na_2SO_4, filtered and evaporated under reduced pressure. Column chromatography (light petroleum/EtOAc, 2:8) of the crude afforded compound **35** as white crystals. Yield**:** 869 mg (52%); R_f = 0.62 (light petroleum/EtOAc, 2:8). ^{1}H NMR (300 MHz, $CDCl_3$): δ = 3.33 (dd, J = 14.3, 10.0 Hz, 1H), 3.50 (dd, J = 14.3, 5.3 Hz, 1H), 3.73 (s, 3H), 5.29 (dd, J = 10.0, 5.3 Hz, 1H), 6.00 (td, J = 6.7, 1.3 Hz, 1H), 6.49 (dd, J = 9.4, 1.3 Hz, 1H), 6.95 (dd, J = 7.0, 1.8 Hz, 1H), 7.03-7.08 (m, 2H), 7.15-7.27 (m, 4H) ppm.

(*S*)-Ethyl 2-(2-oxopyridin-1(2*H*)-yl)-4-phenylbutanoate (36). The synthesis of ester **36** was carried out in agreement with the procedure described for compound **35**, by reacting pyridin-2(1H)-one **26** (799 mg, 8.4 mmol), NaH (336 mg, 8.4 mmol), and (*R*)-1-(ethoxycarbonyl)-3-phenylpropyl methanesulfonate **34** (2 g, 7 mmol). Consistency: yellow oil. Yield: 1.2 g (50%); R_f = 0.61 (light petroleum/EtOAc, 3:7). ^{1}H NMR (300 MHz, $CDCl_3$): δ = 1.24 (t, J = 7.1 Hz, 3H), 2.19-2.34 (m, 1H), 2.45-2.72 (m, 3H), 4.19 (q, J = 7.1 Hz, 2H), 5.50 (dd, J = 9.9, 4.5 Hz, 1H), 6.22 (td, J = 6.3, 1.3 Hz, 1H), 6.59 (dd, J = 9.1, 1.3 Hz, 1H), 7.10-7.39 (m, 7H) ppm.

(*S*)-2-(2-Oxopyridin-1(2*H*)-yl)-3-phenylpropanoic acid (37). A solution of ester **35** (275 mg, 1.07 mmol) in MeOH/H_2O/dioxane (1:1:1) at 0°C was treated with LiOH (128 mg, 5.34 mmol) and stirred for 12h. MeOH and dioxane was evaporated in vacuo and the aqueous solution was treated with 5% citric acid and extracted with EtOAc. The organic layer was dried over Na_2SO_4, filtered and concentrated to afford the acid **37** as a white powder. Yield: 240 mg (92%). $[\alpha]_D^{20}$ = -33.1 (*c* = 0.6, DMSO). ^{1}H NMR (300 MHz, CH_3OH-d_4): δ = 3.45 (dd, J = 14.2, 9.9 Hz, 1H), 3.59 (dd, J = 14.2, 5.2 Hz, 1H), 5.37 (dd, J = 9.9, 5.2 Hz, 1H), 6.18 (td, J = 6.6, 1.3 Hz, 1H), 6.45 (dd, J = 9.1, 1.3 Hz, 1H), 7.05-7.20 (m, 5H), 7.29-7.33 (m, 1H), 7.37-7.44 (m, 1H) ppm.

(*S*)-2-(2-Oxopyridin-1(2*H*)-yl)-4-phenylbutanoic acid (38). The synthesis of acid **38** was carried out in agreement with the procedure described for compound **37**, by reacting ester **36** (435 mg, 1.52 mmol) and LiOH (182 mg, 7.62 mmol). Consistency: white powder. Yield: 360 mg (89%). $[\alpha]_D^{20}$ = +27.4 (*c* = 0.6, DMSO). ^{1}H NMR (300 MHz, CH_3OH-d_4): δ = 2.35-2.48 (m, 1H), 2.49-2.64 (m, 3H), 5.30 (dd, J = 10.2, 4.1 Hz, 1H), 6.42 (td, J = 6.8, 1.3 Hz, 1H), 6.55 (dd, J = 8.7, 1.3 Hz, 1H), 7.11-7.29 (m, 5H), 7.53 (ddd, J = 8.9, 6.7, 2.0 Hz, 1H), 7.61 (dd, *J* = 6.8, 1.9 Hz, 1H) ppm.

General procedures for the synthesis of amides 12-18 and 19-25 The coupling reactions between the carboxylic acids **37**-**38** (1 equiv.) and the suitable amines (1.5 equiv.) were carried out as above described for

compounds **2-11**. The final compounds were purified by column chromatography, using EtOAc/light petroleum, 8:2 as eluent mixture.

(*S*)-2-(2-Oxopyridin-1(2*H*)-yl)-*N*,3-diphenylpropanamide (12): yield: 44%. R_f = 0.55 (EtOAc/light petroleum, 8:2). ^{1}H NMR (300 MHz, $CDCl_3$): δ = 3.19 (dd, J = 13.8, 7.5 Hz, 1H), 3.65 (dd, J = 13.8, 8.3 Hz, 1H), 6.04 (t, J = 7.8 Hz, 1H), 6.31 (td, J = 7.0, 1.3 Hz, 1H), 6.57 (dd, J = 9.1, 1.3 Hz, 1H), 7.02-7.50 (m, 11H), 7.71 (dd, J = 7.0, 1.5 Hz, 1H), 9.24 (bs, 1H) ppm. ^{13}C NMR: (75 MHz, $CDCl_3$): δ = 36.45, 63.76, 107.26, 119.95, 120.19, 124.45, 127.09, 128.69, 128.87, 129.12, 135.66, 137.63, 140.00, 142.78, 164.81, 166.72 ppm. Elemental analysis: calcd for $C_{20}H_{18}N_2O_2$: C 75.45; H 5.70; N 8.80; found: C 75.56, H 5.65, N 8.95.

(*S*)-*N*-Benzyl-2-(2-oxopyridin-1(2*H*)-yl)-3-phenylpropanamide (13): yield: 48%. R_f = 0.68 (EtOAc/light petroleum, 9:1). ^{1}H NMR (300 MHz, $CDCl_3$): δ = 3.10 (dd, J = 13.5, 6.9 Hz, 1H), 3.52 (dd, J = 13.5, 9.1 Hz, 1H), 4.16 (dd, J = 15.0, 5.1 Hz, 1H), 4.48 (dd, J = 15.0, 6.6 Hz, 1H), 5.91 (t, J = 7.9 Hz, 1H), 6.25 (td, J = 7.0, 1.3 Hz, 1H), 6.33 (dd, J = 9.2, 1.3 Hz, 1H), 6.91-7.01 (m, 2H), 7.16-7.31 (m, 9H), 7.42 (bs, 1H), 7.76 (dd, J = 7.0, 1.3 Hz, 1H) ppm. ^{13}C NMR: (75 MHz, $CDCl_3$): δ = 37.03, 43.43, 53.79, 106.78, 120.02, 127.01, 127.26, 127.38, 128.51, 128.64, 129.24, 134.64, 137.53, 139.62, 141.70, 162.54, 168.51 ppm. Elemental analysis: calcd for $C_{21}H_{20}N_2O_2$: C 75.88; H 6.06; N 8.43; found: C 75.99, H 6.17, N 8.12.

(*S*)-2-(2-Oxopyridin-1(2*H*)-yl)-*N*-phenethyl-3-phenylpropanamide (14): yield: 92%. R_f = 0.63 (EtOAc/light petroleum, 9:1). ^{1}H NMR (300 MHz, $CDCl_3$): δ = 2.54-2.73 (m, 2H), 3.06 (dd, J = 13.7, 7.2 Hz, 1H), 3.24-3.37 (m, 1H), 3.39-3.53 (m, 2H), 5.80 (t, J = 7.9 Hz, 1H), 6.22 (td, J = 7.0, 1.4 Hz, 1H), 6.39 (dd, J = 9.1, 0.8 Hz, 1H), 6.93-7.01 (m, 2H), 7.10 (bs, 1H), 7.13-7.35 (m, 9H), 7.69 (dd, J = 7.0, 1.8 Hz, 1H) ppm. ^{13}C NMR: (75 MHz, $CDCl_3$): δ = 35.37, 36.99, 40.92, 57.71, 106.68, 120.04, 126.34, 127.00, 128.48, 128.60, 128.64, 129.22, 134.67, 135.98, 138.66, 139.59, 162.45, 168.54 ppm. Elemental analysis: calcd for $C_{22}H_{22}N_2O_2$: C 76.28; H 6.40; N 8.09; found: C 76.20, H 6.12, N 8.29.

(*S*)-2-(2-Oxopyridin-1(2*H*)-yl)-3-phenyl-*N*-(3-phenylpropyl)propanamide (15): yield: 84%. R_f = 0.64 (EtOAc/light petroleum, 9:1). ^{1}H NMR (300 MHz, $CDCl_3$): δ = 1.61-1.73 (m, 2H), 2.44 (t, J = 8.4 Hz, 2H), 3.02-3.14 (m, 2H), 3.17-3.29 (m, 1H), 3.50 (dd, J = 13.6, 8.8 Hz, 1H), 5.84 (dd, J = 8.4, 7.5 Hz, 1H), 6.24 (td, J = 7.0, 1.4 Hz, 1H), 6.47 (dd, J = 9.1, 0.8 Hz, 1H), 6.99-7.36 (m, 12H), 7.73 (dd, J = 7.0, 1.8 Hz, 1H) ppm. ^{13}C NMR: (75 MHz, $CDCl_3$): δ = 30.76, 32.88, 36.88, 39.06, 57.80, 106.76, 120.02, 125.90, 127.01, 128.35, 128.60, 129.16, 134,69, 135.92, 139.69, 141.30, 143.72, 162.57, 168.55 ppm. Elemental analysis: calcd for $C_{23}H_{24}N_2O_2$: C 76.64; H 6.71; N 7.77; found: C 76.50, H 6.83, N 7.40.

(*S*)-*N*-Cyclohexyl-2-(2-oxopyridin-1(2*H*)-yl)-3-phenylpropanamide (16): yield: 65%. R_f = 0.64 (EtOAc/light petroleum, 9:1). ^{1}H NMR (300 MHz, $CDCl_3$): δ = 0.90-1.79 (m, 10H), 3.09 (dd, J = 13.6, 7.0 Hz, 1H), 3.48 (dd, J = 13.6, 8.9 Hz, 1H), 3.55-3.71 (m, 1H), 5.78 (dd, J = 8.9, 7.0 Hz, 1H), 6.24 (td, J = 7.0, 1.4 Hz, 1H), 6.50 (dd, J = 9.1, 1.4 Hz, 1H), 6.66 (bs, 1H), 7.14-7.36 (m, 6H), 7.75 (dd, J = 7.0, 1.7 Hz, 1H) ppm. ^{13}C NMR: (75 MHz, $CDCl_3$): δ = 24.57, 25.36, 32.38, 32.52, 37.14, 48.40, 106.55, 119.98, 126.94, 128.55, 129.18, 134.73, 135.95, 139.54, 162.48, 167.54 ppm. Elemental analysis: calcd for $C_{20}H_{24}N_2O_2$: C 74.04; H 7.46; N 8.64; found: C 74.25, H 7.30, N 8.75.

(*S*)-*N*-Butyl-2-(2-oxopyridin-1(2*H*)-yl)-3-phenylpropanamide (17): yield: 47%. R_f = 0.60 (EtOAc/light petroleum, 9:1). ^{1}H NMR (300 MHz, $CDCl_3$): δ = 0.82 (t, J = 7.3 Hz, 3H), 1.06-1.21 (m, 2H), 1.22-1.38 (m, 2H), 2.98-3.13 (m, 2H), 3.14-3.26 (m, 1H), 3.52 (dd, J = 13.6, 8.9 Hz, 1H), 5.78 (t, J = 7.9 Hz, 1H), 6.25 (td, J = 7.0, 1.2 Hz, 1H), 6.52 (dd, J = 9.1, 1.2 Hz, 1H), 6.67 (bs, 1H), 7.14-7.35 (m, 6H), 7.69 (dd, J = 7.0, 1.8 Hz, 1H) ppm. ^{13}C NMR: (75 MHz, $CDCl_3$): δ = 13.64, 19.77, 31.13, 36.70, 39.26, 57.83, 106.73, 120.07, 126.98, 128.60, 129.13, 134.54, 135.91, 139.62, 162.60, 168.38 ppm. Elemental analysis: calcd for $C_{18}H_{22}N_2O_2$: C 72.46; H 7.43; N 9.39; found: C 72.06, H 7.54, N 9.31.

(*S*)-*N*-Isopentyl-2-(2-oxopyridin-1(2*H*)-yl)-3-phenylpropanamide (18): yield: 69%. R_f = 0.57 (EtOAc/light petroleum, 9:1). ^{1}H NMR (300 MHz, $CDCl_3$): δ = 0.80 (d, J = 6.5 Hz, 6H), 1.17-1.42 (m, 3H), 2.99-3.28 (m, 3H), 3.51 (dd, J = 13.6, 8.9 Hz, 1H), 5.78 (t, J = 7.9 Hz, 1H), 6.26 (td, J = 6.9, 1.2 Hz, 1H), 6.53 (dd, J = 9.1, 1.2 Hz, 1H), 6.78 (bs, 1H), 7.14-7.38 (m, 6H), 7.73 (dd, J = 6.9, 1.8 Hz, 1H) ppm. ^{13}C NMR: (75 MHz, $CDCl_3$): δ = 22.34, 25.50, 36.85, 37.86, 39.37, 51.45, 106.87, 120.02, 126.98, 128.58, 129.13, 134.63, 135.85, 139.69, 162.60, 168.34 ppm. Elemental analysis: calcd for $C_{19}H_{24}N_2O_2$: C 73.05; H 7.74; N 8.97; found: C 73.25, H 7.85, N 8.70.

(*S*)-2-(2-Oxopyridin-1(2*H*)-yl)-*N*,4-diphenylbutanamide (19): yield: 50%. R_f = 0.72 (EtOAc/light petroleum, 8:2). ^{1}H NMR (300 MHz, $CDCl_3$): δ = 2.14-2.30 (m, 1H), 2.57-2.77 (m, 3H), 5.61 (t, J = 7.4 Hz, 1H), 6.31 (td, J = 6.8, 1.4 Hz, 1H), 6.66 (d, J = 9.2 Hz, 1H), 7.10 (t, J = 7.4 Hz, 1H), 7.13-7.24 (m, 3H), 7.25-7.35 (m, 4H), 7.39 (ddd, J = 8.9, 6.6, 2.0 Hz, 1H), 7.50-7.58 (m, 3H), 9.11 (bs, 1H) ppm. ^{13}C NMR: (75 MHz, $CDCl_3$): δ = 32.07, 44.13, 47.01, 101.50, 110.00, 119.90, 120.45, 121.81, 128.40, 128.63, 128.96, 136.31, 139.95, 140.07, 142.35, 165.12, 166.54 ppm. Elemental analysis: calcd for $C_{21}H_{20}N_2O_2$: C 75.88; H 6.06; N 8.43; found: C 75.56, H 6.016, N 8.58.

(*S*)-N-Benzyl-2-(2-oxopyridin-1(2*H*)-yl)-4-phenylbutanamide (20): yield: 95%. R_f = 0.63 (EtOAc/light petroleum, 8:2). ^{1}H NMR (300 MHz, $CDCl_3$): δ = 2.07-2.24 (m, 1H), 2.43-2.71 (m, 3H), 4.30 (dd, J = 14.8, 5.3 Hz, 1H), 4.51 (dd, J = 14.8, 6.0 Hz, 1H), 5.60 (t, J = 7.7 Hz, 1H), 6.26 (td, J = 6.8, 1.4 Hz, 1H), 6.48 (d, J = 9.2 Hz, 1H), 7.08-7.36 (m, 11H), 7.43 (bs, 1H), 7.59 (dd, J = 6.8, 1.8 Hz, 1H) ppm. ^{13}C NMR: (75 MHz, $CDCl_3$): δ = 32.04, 32.42, 43.58, 56.29, 107.00, 120.14, 126.32, 127.42, 127.55, 128.35, 128.55, 128.64, 134.31, 137.77, 139.68, 140.24, 162.77, 168.92 ppm. Elemental analysis: calcd for $C_{22}H_{22}N_2O_2$: C 76.28; H 6.40; N 8.09; found: C 76.01, H 6.35, N 8.19.

(*S*)-2-(2-Oxopyridin-1(2*H*)-yl)-*N*-phenethyl-4-phenylbutanamide (21): yield: 92%. R_f = 0.56 (EtOAc/light petroleum, 8:2). ^{1}H NMR (300 MHz, $CDCl_3$): δ = 1.98-2.15 (m, 1H), 2.39-2.66 (m, 3H), 2.68-2.85 (m, 2H), 3.38-3.56 (m, 2H), 5.43 (t, J = 7.8 Hz, 1H), 6.31 (td, J = 6.8, 1.4 Hz, 1H), 6.55 (dd, J = 9.2, 1.4 Hz, 1H), 6.84 (bs, 1H), 7.02-7.38 (m, 11H), 7.50 (dd, J = 6.8, 1.4 Hz, 1H) ppm.^{13}C NMR: (75 MHz, $CDCl_3$): δ = 32.00, 32.09, 35.48, 40.77, 56.63, 106.96, 120.27, 126.31, 126.45, 127.5, 128.34, 128.54, 128.64, 134.09, 138.52, 139.57, 140.27, 162.69, 168.81 ppm. Elemental analysis: calcd for $C_{23}H_{24}N_2O_2$: C 76.64; H 6.71; N 7.77; trov: C 76.34, H 6.81, N 7.50.

(*S*)-2-(2-Oxopyridin-1(2*H*)-yl)-4-phenyl-*N*-(3-phenylpropyl)butanamide (22): yield: 67%. R_f = 0.53 (EtOAc/light petroleum, 8:2). ^{1}H NMR (300 MHz, $CDCl_3$): δ = 1.68-1.88 (m, 2H), 2.06-2.22 (m, 1H), 2.41-2.74 (m, 5H), 3.10-3.33 (m, 2H), 5.48 (t, J = 7.7 Hz, 1H), 6.26 (td, J = 6.8, 1.4 Hz, 1H), 6.58 (dd, J = 9.2, 1.4 Hz, 1H), 6.93 (bs, 1H), 7.03-7.41 (m, 11H), 7.55 (dd, J = 6.8, 2.1 Hz, 1H) ppm. ^{13}C NMR: (75 MHz, $CDCl_3$): δ = 31.98, 30.99, 32.04, 33.04, 39.12, 56.45, 107.08, 120.24, 125.97, 126.36, 128.37, 128.43, 128.57, 130.81, 134.14, 139.72, 140.26, 140.91, 165.48, 168.86 ppm. Elemental analysis: calcd for $C_{24}H_{26}N_2O_2$: C, 76.98; H, 7.00; N, 7.48; found: C 76.68, H 7.32, N 7.28.

(*S*)-*N*-Cyclohexyl-2-(2-oxopyridin-1(2*H*)-yl)-4-phenylbutanamide (23): yield: 89%. R_f = 0.56 (EtOAc/light petroleum, 8:2). ^{1}H NMR (300 MHz, $CDCl_3$): δ = 0.97-1.80 (m, 10H), 2.03-2.24 (m, 1H), 2.38-2.72 (m, 3H), 3.58-3.78 (m, 1H), 5.47 (t, J = 7.4 Hz, 1H), 6.24 (td, J = 6.8, 1.4 Hz, 1H), 6.58 (dd, J = 9.2, 1.4 Hz, 1H), 6.65 (bs, 1H), 7.09-7.41 (m, 6H), 7.57 (dd, J = 6.8, 1.8 Hz, 1H) ppm. ^{13}C NMR: (75 MHz, $CDCl_3$): δ = 24.70, 25.40, 32.06, 32.56, 32.81, 48.48, 56.35, 106.84, 120.07, 126.28, 128.34, 128.52, 134.38, 139.60, 140.36, 162.69, 167.91 ppm. Elemental analysis: calcd for $C_{21}H_{26}N_2O_2$: C 74.52; H 7.74; N 8.28; found: C 74.59, H 7.60, N 8.39.

(*S*)-N-Butyl-2-(2-oxopyridin-1(2*H*)-yl)-4-phenylbutanamide (24): yield: 51%. R_f = 0.57 (EtOAc/light petroleum, 8:2). ^{1}H NMR (300 MHz, $CDCl_3$): δ = 0.87 (t, J = 7.2 Hz, 3H), 1.18-1.35 (m, 2H), 1.37-1.54 (m, 2H), 2.03-2.21 (m, 1H), 2.40-2.72 (m, 3H), 3.05-3.34 (m, 2H), 5.53 (t, J = 7.6 Hz, 1H), 6.26 (td, J = 6.7, 1.4 Hz, 1H), 6.57 (dd, J = 9.2, 1.4 Hz, 1H), 6.95 (bs, 1H), 7.07-7.41 (m, 6H), 7.59 (dd, J = 6.7, 1.8 Hz, 1H) ppm. ^{13}C NMR: (75 MHz, $CDCl_3$): δ =13.70, 19.97, 31.30, 32.06, 32.65, 39.34, 56.25, 106.88, 119.99, 126.26, 128.32, 128.51, 134.50, 139.68, 140.35, 162.72, 168.87 ppm. Elemental analysis: calcd for $C_{19}H_{24}N_2O_2$: C 73.05; H 7.74; N 8.97; found: C 72.95, H 7.85, N 8.81.

(*S*)-*N*-Isopentyl-2-(2-oxopyridin-1(2*H*)-yl)-4-phenylbutanamide (25): yield: 37%. R_f = 0.55 (EtOAc/light petroleum, 8:2). ^{1}H NMR (300 MHz, $CDCl_3$): δ = 0.86 (d, J = 6.6 Hz, 6H), 1.16-1.46 (m, 3H), 2.04-2.25 (m, 1H), 2.40-2.73 (m, 3H), 3.09-3.35 (m, 2H), 5.44 (t, J = 7.6 Hz, 1H), 6.25 (td, J = 6.7, 1.3 Hz, 1H), 6.59 (dd, J = 9.2, 1.4 Hz, 1H), 6.76 (bs, 1H), 7.06-7.43 (m, 6H), 7.59 (dd, J = 6.7, 1.8 Hz, 1H) ppm. ^{13}C NMR: (75 MHz, $CDCl_3$): δ =22.35, 22.40, 25.77, 32.03, 32.27, 37.98, 38.04, 56.34, 107.08, 120.13, 126.31, 128.34, 128.54, 134.25, 139.72, 140.27, 162.80, 168.72 ppm. Elemental analysis: calcd for $C_{20}H_{26}N_2O_2$: C 73.59; H 8.03; N 8.58; found: C 73.79, H 8.24, N 8.41.

In vitro 20S immunoproteasome/proteasome inhibition assays

Human 20S immunoproteasome, obtained from human spleen, and human 20S proteasome, isolated from human erythrocytes, were purchased from Enzo Life Science. The hydrolysis of the appropriate peptidyl 7-amino-4-methyl-coumarin substrate was monitored to measure the different proteolytic activities of both proteasome and immunoproteasome. The substrates Suc-Leu-Leu-Val-Tyr-AMC (Bachem) for β5c-β5i, Boc-Leu-Arg-Arg-AMC (Bachem) for β2c-β2i, Z-Leu-Leu-Glu-AMC (Adipogen) for β1c and Ac-Pro-Ala-Leu-AMC (Biomol GmbH) for β1i subunits were employed at 50 μM, with the exception of Z-Leu-Leu-Glu-AMC (80 μM). Fluorescence of the product AMC of the substrate hydrolyses was measured at 30°C with a 380 nm excitation filter and a 460 nm emission filter, using an Infinite 200 PRO microplate reader (Tecan, Männedorf, Switzerland). A preliminary screening at 50 μM inhibitor concentrations was carried out on the three proteolytic activities of proteasome and immunoproteasome; an equivalent amount of DMSO as a negative control and MG-132 (a reversible inhibitor of immunoproteasome) as positive control were employed. Compounds showing at least 60% inhibition at the screening concentration were then progressed into detailed assays. Continuous assays were performed at seven different concentrations ranging from those that minimally inhibited to those that fully inhibited each proteolytic activity to calculate the dissociation constants K_i of the enzyme-inhibitor complex by means of the Cheng-Prusoff equation $K_i = IC_{50}/(1 + [S]\ K_m^{-1})$. Inhibitor solutions were prepared from stocks in DMSO. Each independent assay was performed in duplicate in 96-well-plates in a total volume of 200 μL. For the assay on β5i, β1i, β1c and β5c subunits, human 20S immunoproteasome or human 20S proteasome was incubated at 30°C obtaining a final concentration of 0.004 mg/mL with the inhibitor at seven different concentrations. The reaction buffer comprised: 50 mM Tris HCl, pH 7.4, 25 mM KCl, 10 mM NaCl, 1 mM $MgCl_2$, 0.03% SDS. AMC released from substrate hydrolysis was monitored in kinetic cycle over a period of 10 min. For the assay on β2i and β2c subunits, final concentration of immunoproteasome or proteasome was of 0.0025 mg/mL. The reaction buffer comprised: 50 mM Tris HCl, pH 7.4, 0.5 mM EDTA III, 50 mM NaCl, 0.03% SDS.

Computational details & methodology

Protein and ligand preparation

Since the only available crystal structures of the human i20S are yeast chimera that incorporate key parts of human β5i and the neighboring β6 subunit but are devoid of the β1i subunit,[34] we employed the crystal structure of the murine i20S in complex with the inhibitor PR-957 (PDB ID: 3UNF)[7] for docking studies. Murine and human 20S subunits share a sequence identity of more than 90%, and the few non-identical residues are external to the active sites.

For docking purpose, we selected the catalytic subunits β1i (LMP2, *PSMB9*)/β2i (MECL-1, *PSMB10*) and β5i (LMP7, *PSMB8*)/β6i. The crystal structure of PR-957 bound to β1i revealed two well-defined water molecules within the S3 pocket, which coordinate a tight H-bond network between β1i-A50N, β2i-S118O$^\gamma$ and the carbonyl oxygen and the amide nitrogen of PR-957 P3 alanine, respectively. Accordingly, the intervening water molecules were included in the docking experiments. The protein setup was carried out using the Protein Preparation Wizard implemented in Maestro 11.3 (Schrödinger, LLC, New York, NY, 2018). Hydrogen atoms were added to the protein consistent with the neutral physiologic pH. Arginine and lysine side chains were considered as cationic at the guanidine and ammonium groups, and the aspartic and glutamic residues were considered as anionic at the carboxylate groups. The protonation and flip states of the imidazole rings of the histidine residues were adjusted together with the side chain amides of glutamine and asparagine residues in a H-bonding network optimization process. Successively, the protein hydrogen atoms only were minimized using the Impref module of Impact with the OPLS_2005 force field.

Initial coordinates of compounds **1**, **7**, **13** and **21** were constructed by using the Molecular Builder module in Maestro. The structures were energy-minimized using Macromodel 10.8 (Schrödinger, LLC, New York, NY, 2018) using the MMFF force field with the steepest descent (1000 steps) followed by truncated Newton conjugate gradient (500 steps) methods. Partial atomic charges were computed using the OPLS-AA force field.

Molecular Docking

Docking of compounds **1**, **7**, **13** and **21**into the active site of β1i or β5i was performed with the genetic algorithm implemented in GOLD 5.5 (CCDC Software Limited: Cambridge, U.K., 2008).[29] The coordinates of the cocrystallized ligand PR-957, in β1i and β5i respectively, were chosen as active-site origin. The active-site radius was set equal to 10 Å. Explicit water molecules were allowed to toggle on or off during the individual docking runs (i.e., these waters were not automatically present in the binding site, but were included if their presence strengthened the interaction of the ligand with the receptor, as determined by the scoring function).[37] Orientation mode of water hydrogen atoms was set to "spin". We adopted all the program default parameters: for each molecule tested the number of islands was set to 5, population size to 100, number of operations was 100,000 with a selective pressure of 1.1. For these experiments, the number of GA runs was set to 200 without the option of early termination, and scoring of the docked poses was performed with the original ChemPLP scoring function rescoring with ChemScore.[38] The final receptor-ligand complex for each ligand was chosen interactively by selecting the highest scoring pose that was consistent with the experimentally derived information about the binding mode of the ligand. Figures were prepared using Pymol (Schrödinger, LLC, New York, NY, 2018). All computations were performed on an E4 Computer Engineering E1080 workstation provided with an Intel Xeon processor.

Acknowledgements

S.M. acknowledges the support of "Programma Operativo Fondo Sociale Europeo (FSE) Regione Siciliana 2014–2020 – Asse 3 Ob. 10.5" for her PhD fellowship. A.L. thanks "Combattere la resistenza tumorale: piattaforma integrata multidisciplinare per un approccio tecnologico innovativo alle oncoterapie-CAMPANIA ONCO TERAPIE" of Regione Campania (Italy) for partial support of this work.

Keywords: Immunoproteasome •Amide derivatives • Non-covalent inhibitors • Docking studies•

References:

[1] S. H. Lecker, A. L. Goldberg, W. E. Mitch, *JASN* **2006**, *17,* 1807-1819.
[2] G. N. De Martino, T. G. Gillette, *Cell*, **2007**, *129*, 659–662.
[3] N. Micale, K. Scarbaci, V. Troiano, R. Ettari, S. Grasso, M. Zappalà, *Med. Res. Rev.*, **2014**, *34*, 1001-1069.
[4] A. Ciechanover, A. L. Schwartz, *Biochim. Biophys. Acta*, **2004**, *1695*, 3-17
[5] A. F. Kisselev, W.A. van der Linden, H. S. Overkleeft, *Chem. Biol.*, **2012**, *19*, 99–115.
[6] M. Groll, L. Ditzel, J. Lowe, D. Stock, M. Bochtler, H.D. Bartunik, R. Huber, *Nature*. **1997**, *386*, 463–471.
[7] E.M. Huber, M. Basler, R. Schwab, W. Heinemeyer, C.J. Kirk, M. Groettrup, M. Groll, Cell **2012**, *148*, 727–738.
[8] R. Ettari, S. Previti, A. Bitto, S. Grasso, M. Zappalà, *Curr. Med. Chem.* **2016**, *23*, 1217-1238.
[9] D. J. Kuhn, R. Z. Orlowski, *Semin. Hematol.*, **2012**, *49*, 258-262.
[10] E. M. Huber, M. Groll, *Angew. Chem. Int. Ed. Engl*. **2012**, *51*, 8708–8720
[11] R. Ettari, M. Zappalà, S. Grasso, C. Musolino, V. Innao, A. Allegra, *Pharmacol. Ther*. **2018**, *182*, 176-192.
[12] G. de Bruin, E. M. Huber, B.-T. Xin, E. J. van Rooden, K. Al-Ayed, K.-B. Kim, A. F. Kisselev, C. Driessen, M. van der Stelt, G. A. van der Marel, M. Groll, H. S. Overkleeft *J. Med. Chem.* **2014** *57*, 6197-6209
[13] H. W. B. Johnson, J. L. Anderl, E. K. Bradley, J. Bui, J. Jones, S. Arastu-Kapur, L. M. Kelly, E. Lowe, D. C. Moebius, T. Muchamuel, C. Kirk, Z. Wang, D. L. McMinn *ACS Med. Chem. Lett.* **2017,** *8*, 413-417.
[14] H. W. B. Johnson, E. Lowe, J. L. Anderl, A. Fan, T. Muchamuel, S. Bowers, D. C. Moebius, C. Kirk, D. L.McMinn *J. Med. Chem.* **2018,** *61*, 11127-11143.
[15] M. Kaiser, M. Groll, C. Siciliano, I. Assfalg-Machleidt, E. Weyher, J. Kohno, A. G. Milbradt, C. Renner, R. Huber, L. Moroder. *ChemBioChem,* **2004**, *5*, 1256-1266.
[16] M. Groll, N. Gallastegui, X. Maréchal, V. Le Ravalec, N. Basse, N. Richy, E. Genin, R. Huber, L. Moroder, J. Vidal, M. Reboud-Ravaux. *ChemMedChem*, **2010**, *5*, 1701-1705.
[17] N. Gallastegui, P. Beck, M. Arciniega, R. Huber, S. Hillebrand, M. Groll. *Angew Chem Int Ed Engl.* **2012**, 51, 247-249.
[18] R. L. A. Santos, L. Bai, P. K. Singh, N. Murakami, H. Fan, W. Zhan, Y. Zhu, X. Jiang, K. Zhang, J. P. Assker, C. F. Nathan, H. Li, J. Azzi, G. Lin. *Nat Commun.,* **2017**, 8, 1692.
[19] R. Ettari, C. Bonaccorso, N. Micale, C. Heindl, T. Schirmeister, M.L. Calabrò, S. Grasso, M. Zappalà, *ChemMedChem*. **2011**, *6*, 1228–1237.
[20] N. Micale, R. Ettari, A. Lavecchia, C. Di Giovanni, K. Scarbaci, V. Troiano, S. Grasso, E. Novellino, T. Schirmeister, M. Zappalà, *Eur J. Med. Chem*. **2013**, *64*, 23–34.
[21] K. Scarbaci, V. Troiano, N. Micale, R. Ettari, L. Tamborini, C. Di Giovanni, C. Cerchia, S. Grasso, E. Novellino, T. Schirmeister, A. Lavecchia, M. Zappalà, *Eur. J. Med. Chem*. **2014**, *76*, 1–9.
[22] V. Troiano, K. Scarbaci, R. Ettari, N. Micale, C. Cerchia, A. Pinto, T. Schirmeister, E. Novellino, S. Grasso, A. Lavecchia, M. Zappalà,. *Eur. J. Med. Chem.* **2014**, *83*, 1–14.
[23] K. Scarbaci, V. Troiano, R. Ettari, A. Pinto, N. Micale, C. Di Giovanni, C. Cerchia, T. Schirmeister, E. Novellino, A. Lavecchia, M. Zappalà, S. Grasso, *ChemMedChem*. **2014**, *9*, 1801–1816.
[24] C. Di Giovanni, R. Ettari, S. Sarno, A. Rotondo, A. Bitto, F. Squadrito, D. Altavilla, T. Schirmeister, E. Novellino, S. Grasso, M. Zappalà, A. Lavecchia, *Eur. J. Med. Chem.* **2016**, *121*, 578–591.
[25] P. S. Dragovich, T. J. Prins, R. Zhou, T. O. Johnson, Y. Hua, H. T. Luu, S. K. Sakata, E.L. Brown, F. C. Maldonado, T. Tuntland, C. A. Lee, S. A. Fuhrman, L. S. Zalman, A. K. Patick, D. A. Matthews, E. Y. Wu, M. Guo, B. C. Borer, N. K. Nayyar, T. Moran, L. Chen, P. A. Rejto, P. W. Rose, M. C. Guzman, E. Z. Dovalsantos, S. Lee, K. McGee, M. Mohajeri, A. Liese, J. Tao, M. B. Kosa, B. Liu, M. R. Batugo, J. P. Gleeson, Z. P. Wu, J. Liu, J. W. Meador, R. A. Ferre. *J. Med. Chem.* **2003,** *46,* 4572-4585.
[26] E. Verissimo, N. Berry, P. Gibbons, M. L. Cristiano, P. J. Rosenthal, J. Gut, S. A. Ward, P. M. O'Neill. *Bioorg. Med. Chem. Lett.* **2008,** 18, 4210-4214.
[27] P. Sjö, *Fut. Med. Chem.* **2012**, *4*, 651–660.
[28] E. Genin, M. Reboud-Ravaux, J. Vidal, *Curr. Top. Med. Chem.* **2010**, *10*, 232-256.
[29] G. Jones, P. Willett, R.C. Glen, A. R. Leach, R. Taylor, *J. Mol. Biol.* **1997***, 267*, 727-748.
[30] J. Schrader, F. Henneberg, R. A. Mata, K. Tittmann, T.R. Schneider, H. Stark, G. Bourenkov, A. Chari. *Science* **2016**, *353,* 594-598.
[31] G. A. Jeffrey. An introduction to hydrogen bonding, Oxford University Press, New York, **1997**.
[32] E. A. Meyer, R. K. Castellano, F. Diederich, *Angew. Chem. Int. Ed.* **2003**, *42*, 1210–1250.
[33] E. Persch, O. Dumele, F. Diederich, *Angew. Chem. Int. Ed.* **2015**, *54*, 3290–3327.
[34] E. M. Huber, W. Heinemeyer, G. de Bruin, H.S. Overkleeft, M. Groll, *EMBO J*. **2016**, *35*, 2602–2613
[35] F. Parlati, S. J. Lee, M. Aujay, E. Suzuki, K. Levitsky, J. B. Lorens, D. R. Micklem, P. Ruurs, C. Sylvain, L. Lu, K. D. Shenk, M. K. Bennet, *Blood*. **2009**,*114*, 3439–3447.
[36] A. V. Singh, M. Bandi, M. A. Aujay, C. J. Kirk, D. E. Hark, N. Raje, D. Chauhan, K. C. Anderson, *Br. J. Haematol*. **2011**, *152*, 155−163.
[37] M. L. Verdonk, G. Chessari, J. C. Cole, M. J. Hartshorn, C. W. Murray, J. W. M. Nissink, R. D. Taylor, R. Taylor, J. Med. Chem. 2005, 48, 6504–6515.
[38] M.L. Verdonk, J.C. Cole, M.J. Hartshorn, C.W. Murray, R.D. Taylor, Proteins 2003, 52, 609–623.

Entry for the Table of Contents

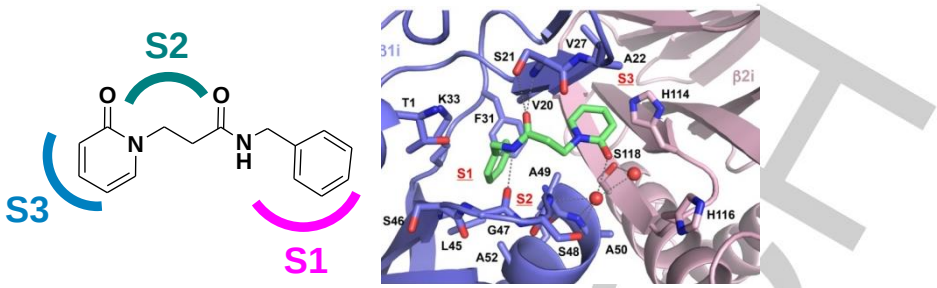

Immunoproteasome inhibitors: the aim of this research was the identification of new immunoproteasome inhibitors. Among the synthesized derivatives, we identified a lead compound able to selectively inhibit β1i subunit of immunoproteasome. Docking studies clarified the binding mode in the catalytic site of immunoproteasome subunits, thus explaining the preferential inhibition of immunoproteasome with respect to proteasome.